International Journal of Civil and Structural Engineering Research ISSN 2348-7607 (Online)
Vol. 13, Issue 1, pp: (84-96), Month: April 2025 - September 2025, Available at: www.researchpublish.com

The Behavior of Ferro-Cement Slabs Reinforced with FRP Bars and Mixed with Seawater under Flexural Loading

Ahmed K. Dagher [1], Khaled Samy [2], Hesham A. Haggag [3], Ahmed M. Ahmed[4,5,6]

[1] M.Sc. Student, Civil Engineering Department, Faculty of Engineering at Mataria, Helwan University, Cairo, Egypt

[2] Assistant Professor, Civil Engineering Department, Higher institute of Engineering and Technology in FifthSettlement, Cairo, Egypt

[3] Professor, Civil Engineering Department, Faculty of Engineering at Mataria, Helwan University, Cairo, Egypt

[4] Assistant Professor, Department of Civil Engineering, Faculty of Engineering at Mataria, Helwan University, Cairo, Egypt

[5] Assistant Professor, Civil & Construction Engineering, School of Engineering & Applied Science, SESC Research Center, Nile University, Giza, Egypt

[6] Smart Engineering Systems Research Center (SESC), Nile University, Giza, Egypt

DOI: https://doi.org/10.5281/zenodo.17018936

Published Date: 01-September-2025

***Abstract*: Ferrocement is a mortar that incorporates wire mesh or bars within a cement mortar structure. This study examines the flexural performance of ferrocement slabs, which were prepared using both potable water and seawater and reinforced with glass fiber bars (GFRP). The research primarily encompasses the impact of the seawater-to-potable water ratio, where seawater content is gradually increased while limiting potable water in five different mortar mixtures. Additionally, various longitudinal reinforcement ratios are analyzed.**

The study encompasses an evaluation of fresh mortar properties, including the mechanical specifications of compressive strength. Furthermore, the flexural behavior of seven one-way slabs is examined. The results indicate that the inclusion of seawater in the mixing water led to an increase in early-age compressive strength. However, increasing seawater content did not have a notable impact on failure behavior. It did lead to a significant reduction in cracking load, with a minor change in failure load, as well as deflection results and fiber and mortar stresses.

Conversely, different longitudinal reinforcement ratios had the opposite effect. The use of 0.37% and 1.25% longitudinal reinforcement was inversely related to crack width and deflection while being directly correlated with cracking load. Similar trends were observed for failure load.

Keywords: **Ferrocement; High-performance mortar; GFRP Bars; Flexural behavior; Seawater.**

1. INTRODUCTION

Experimental Program

1.1 Materials

1.1.1 Cement

Sulfate-resistant cement (SRC) with a grade of 42.5 N was used as a binder in all specimens. The physical and mechanical properties of the cement shown in Table 1 were tested according to B.S EN 197-1 [21]. These specimens exhibited a soundness of 1 mm, compressive strength of 23.1 MPa at 2 days and 50.2 MPa at 28 days, and flexural strength of 4.9 MPa at 2 days and 9.6 MPa at 28 days.

Table 1 Physical and mechanical properties of SRC

Property	Test result
Soundness (mm)	1
Compressive strength 2 days (MPa)	23.1
Compressive strength 28 days (MPa)	50.2
Flexure strength 2 days (MPa)	4.9
Flexure strength 28 days (MPa)	9.6

1.1.2 Fine Aggregate

The fine aggregate used in this research consisted of natural siliceous sand passing a No. 4 sieve (4.75 mm), clean and free of any deleterious substances. As presented in Table 2, the sand has a specific gravity of 2.6, bulk density of 1.63 t/m³, fineness modulus of 2.26, and a soundness of 0.33. The aggregate was graded in conformity with the guide for the design of ferrocement elements [3].

Table 2 Physical properties of sand

Property	Test result	Test Standard
Specific gravity	1	EN 1097-6 [24]
Bulk density (t/m3)	23.1	EN 1097-3 [25]
Fineness modules	50.2	BS EN 933-1 [26]
Soundness (%)	4.9	ASTM C88 [27]

1.1.3 Mixing Water

Two types of water were used: potable water (PW), which is clean drinking water, and seawater (SW), collected from the Red Sea using a pump and a movable tank. A seawater sample was analyzed chemically, and its properties are listed in **Table 3**.

Table 3 Chemical analysis of seawater

Property	Test result
PH	7.8
Electrical conductivity (EC) (µS/cm)	73100
Calcium (mg/l)	400
Magnesium (mg/l)	1773.9
Sodium (mg/l)	12750
Potassium (mg/l)	510
Carbonate (mg/l)	-
Bicarbonate (mg/l)	170.8
Sulphate (mg/l)	8000
PH	7.8

1.1.4 Admixtures

Polypropylene(PP) fibers (12 mm length, 18 µm diameter) were used to reduce shrinkage and cracking. Silica fume(SF) (0.1 µm, 300 kg/m³) was added to enhance mortar strength. Sikament 163M superplasticizer(SP) (1.2 kg/m³) was used to maintain workability at low water-to-cement ratios.

1.1.5 Glass fiber reinforcement rebars (GFRP)

Fiberglass rebars with 8 mm diameter were used for reinforcing all slabs in both longitudinal and transverse directions. As per the results indicated in **Table 4**, the tensile strength of the GFRP bar is 1293 MPa. The test was conducted according to ASTM C1116 [22] with the configuration shown in **Figure 1**.

Table 4 Properties of GFRP rebar

Property	Test result
Density (gm/m3)	1810
Ultimate Stress (MPa)	1293
Strain(mm/mm)	0.03

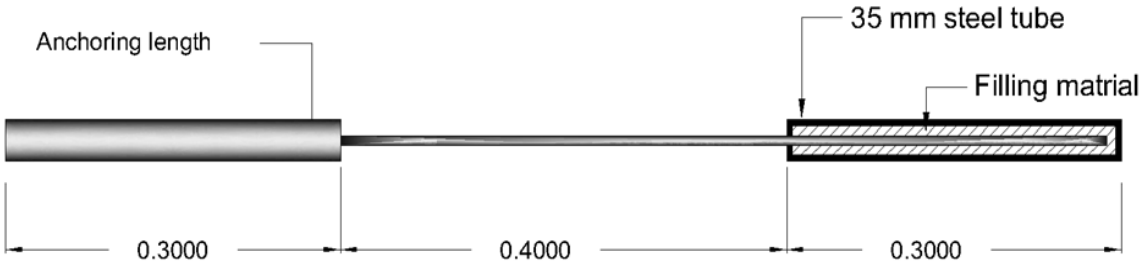

Figure 1 GFRP test sample

Mix Proportions and Testing

As shown in Table 5,the ferrocement mortar was designed for a 28-day compressive strength of 40 MPa using five mixtures with a fixed binder (SRS + SF)-to-sand-to-water ratio of 1:2:0.35, containing 696 kg/m³ binder (626.4 kg/m³ SRS and 69.6 kg/m³ SF, 10% of binder) and 1392 kg/m³ sand. Superplasticizer (1.5% of binder, 10.44 kg/m³) improved workability, while polypropylene fibers (1.5 kg/m³) minimized shrinkage cracks. The total water content was kept at 243.6 kg/m³, with varying proportions of potable water (PW) and seawater (SW) across mixes: Mix 1 (100% PW, 0% SW), Mix 2 (75% PW, 25% SW), Mix 3 (50% PW, 50% SW), Mix 4 (25% PW, 75% SW), and Mix 5 (0% PW, 100% SW).

Table 5 Mixtures Proportions (kg/m3)

Mix ID	Cement (kg)	Silica Fume (kg)	Sand (kg)	Potable Water (kg)	Seawater (kg)	Superplasticizer (kg)	Polypropylene (kg)
M1	626.4	69.6	1392	243.6	0	10.44	1.5
M2	626.4	69.6	1392	182.7	60.9	10.44	1.5
M3	626.4	69.6	1392	121.8	121.8	10.44	1.5
M4	626.4	69.6	1392	60.9	182.7	10.44	1.5
M5	626.4	69.6	1392	0	243.6	10.44	1.5

Initial slump tests were conducted for each mixture, which was then cast into six 100 mm cubic molds and three 150×300 mm cylindrical specimens. After 24 hours, the specimens were water-cured and tested cubes for compressive strength at 7 days, and cylinders for splitting tensile strength at 7 and 28 days as shown in Figure 3 and **Figure 2**. The graphical representation in **Figure 5** shows that seawater slightly reduced slump values, with mixtures M3, M4, and M5 decreasing by 1.81%,4.54%, and 7.27%, respectively, compared to the control (M1). Figure 4 indicates that seawater marginally improved tensile strength, with mixtures M3 and M4 showing a 1.3% increase in failure load and M5 achieving a 3.3% gain compared to the control (M1), while M2 remained nearly unchanged. Figure demonstrates comparable compressive strength development at 7/28 days between seawater and potable water mixtures, with minor fluctuations indicating negligible performance differences. That said, it is also obvious from **Figure 6** that the increase of the seawater ratio with respect to the potable water slightly enhanced the compressive strength at 28 days by a max of 4% in M5 compared to M1.

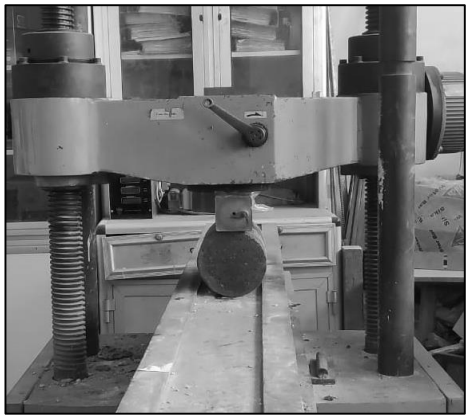

Figure 3 Splitting tensile strength test

Figure 2 Compression test setup

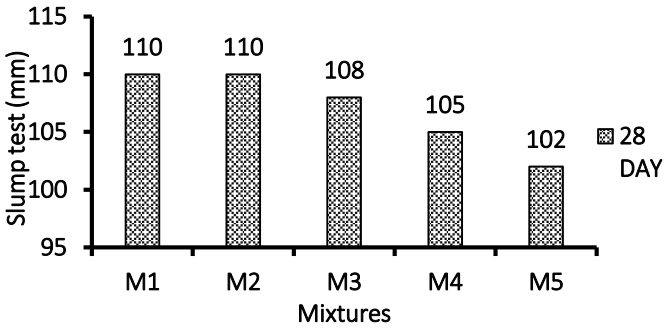

Figure 5 Slump test result for all mixtures

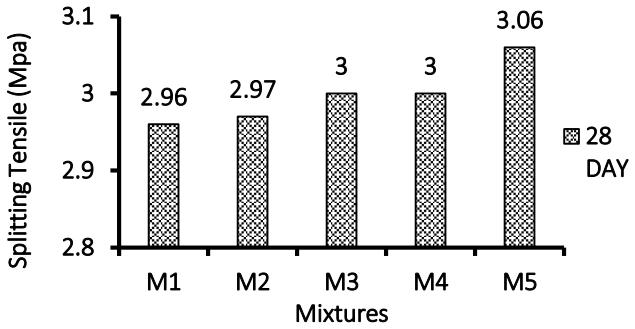

Figure 4 Tensile strength for all mixtures

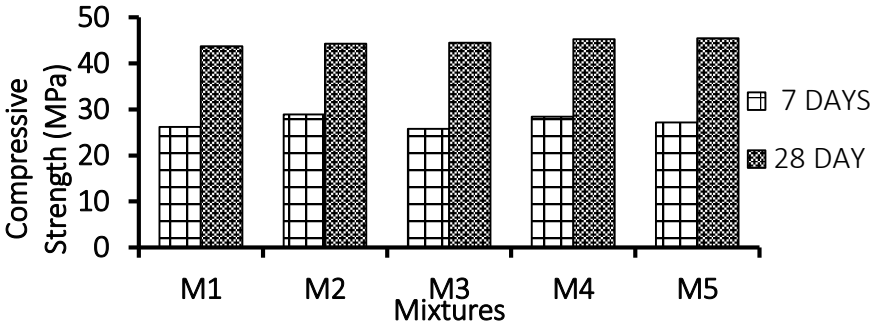

Figure 6 Compressive strength of mortar at 7 and 28 days

Table 6 Percentage increase in the 28-day strength

Mix ID	28-day Compressive strength (MPa)	% difference [(M*-M1)/M1 x100]
M1	43.7	-
M2	44.3	1.4 %
M3	44.5	1.8 %
M4	45.2	3.5 %
M5	45.5	4 %

M* ≡ M1 to M5

1.2 Slabs Description

Seven one-way slabs were tested to evaluate the flexural behavior of ferrocement mortar using different seawater ratios and reinforcement configurations. All slabs measured 1600 mm in length, 500 mm in width, and 100 mm in thickness, with FRP bars placed only in the bottom layer and a 20 mm concrete cover. The slabs were designed according to ECP 208 guidelines. GROUP I (S1–S5) investigated varying seawater-to-potable water ratios using 6Ø8 longitudinal bars, while GROUP II (S6, S7) focused on different reinforcement ratios with 3Ø8 and 10Ø8 bars, respectively. Slab S5 served as a reference for GROUP II and was shared between both groups. The transverse reinforcement for all slabs was 5Ø8/m. The parameters and setup of both groups are illustrated in Figures (7-9).

Table 7 Details of test specimens

Group Name	Slab ID	Mix ID	Bottom Reinforcement		Reinforcement Ratio (%)
			Longitudinal	Transverse	
GROUP I	S1 [Reference]	M1	6Φ8	5Φ8/ m	0.75%
	S2	M2			
	S3	M3			
	S4	M4			
	S5	M5			
GROUP II	S5 [Reference]	M5	6Φ8	5Φ8/ m	0.75%
	S6	M5	3Φ8		0.37%
	S7	M5	10Φ8		1.25%

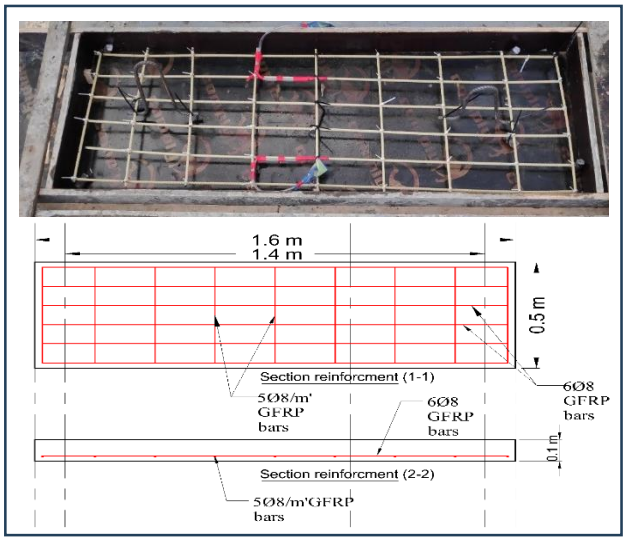

Figure 8 Slabs dimensions and reinforcement details of GROUP I

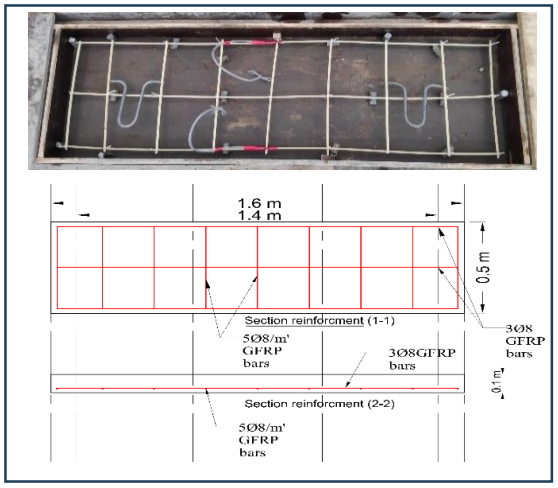

Figure 7 Slab dimensions and reinforcement details of S6

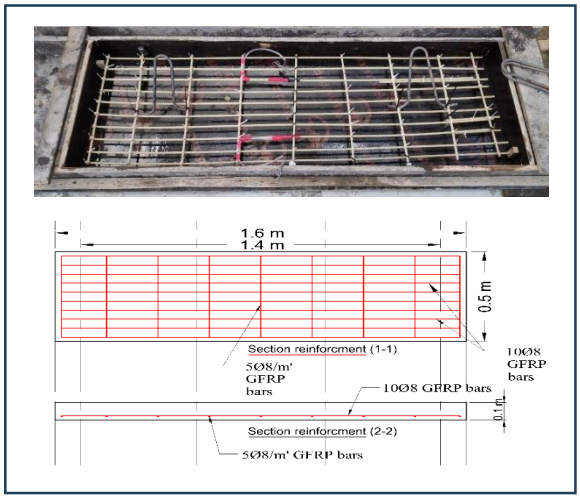

Figure 9 Slab dimensions and reinforcement details of S7

1.3 Test Setup and Procedure.

The test setup shown in **Figure 11** involved using a hydraulic jack with a 500-ton capacity to apply one-third-point loading on the specimens, supported by a reaction frame. Oil pressure was maintained through a pumping unit. A steel beam distributed the load from the load cell into two equal loads ([P/2]) applied on a slab supported 1400 mm apart. The loads were placed 450 mm away from the supports.**Figure 10** express how the bending moment and shear force diagrams determined the strain actions. The test proceeded at 0.2 tons per minute until specimen failure. Instruments like LVDTs and strain gauges measured slab deflection and material strain, with all data recorded through a data acquisition system. Post-failure, cracks were marked to study their distribution and failure patterns.

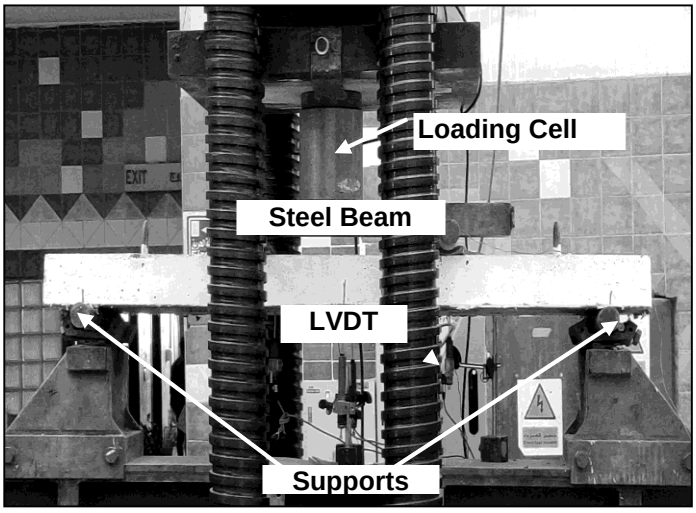

Figure 11 Test setup

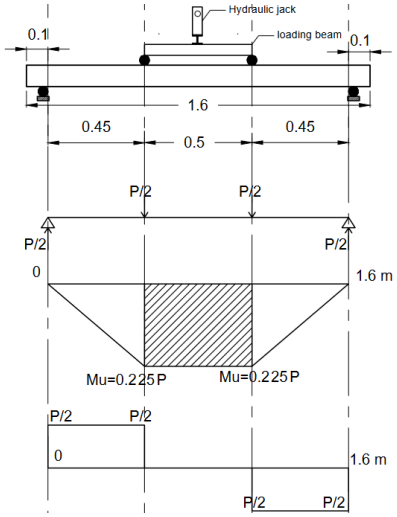

Figure 10 Straining actions on slabs

1.4 Instrumentation

1.4.1 Linear Variable Differential Transformer (LVDT)

The linear variable differential transformer (LVDT) was used in all specimens to measure vertical deflections. A total of four LVDTs were used in each slab. At the mid-span, two LVDTs were placed along the width of the slab to ensure the accuracy of measurements. Two more LVDTs were fixed at the locations of the two concentric loads [P/2, as illustrated in **Figure 10**], where the first one was distant by 450 mm from the right support and the second LVDT had the same distance from the left support. The redundancy of the LVDTs was made to ensure accurate measurements of the deflection during the test. The locations of the LVDTs are shown in **Figure 12**.

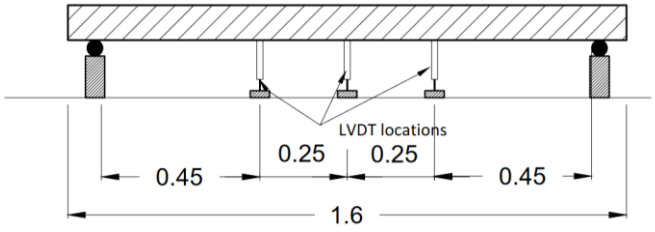

Figure 12 LVDT locations

1.4.2 Strain Gauge

Uniaxial strain gauges were used to measure the strain generated in slabs during testing. Two sizes of strain gauges were used depending on the attached surface. The first had a size of 60 mm, which was used to measure the strain in the concrete. The strain gauge was attached to the top surface of the slab at the mid-span as illustrated in **Figure 13**a. The schematics represented in Figure 13b-13d show the locations of the second size of the strain gauges used in this investigation. That size was 10 mm, which was adopted to measure the strain in the FRP bars. For each slab, two gauges were attached to the FRP bars at the mid-span, and variant in the distance along the width which depended on the arrangement of the FRP bars.

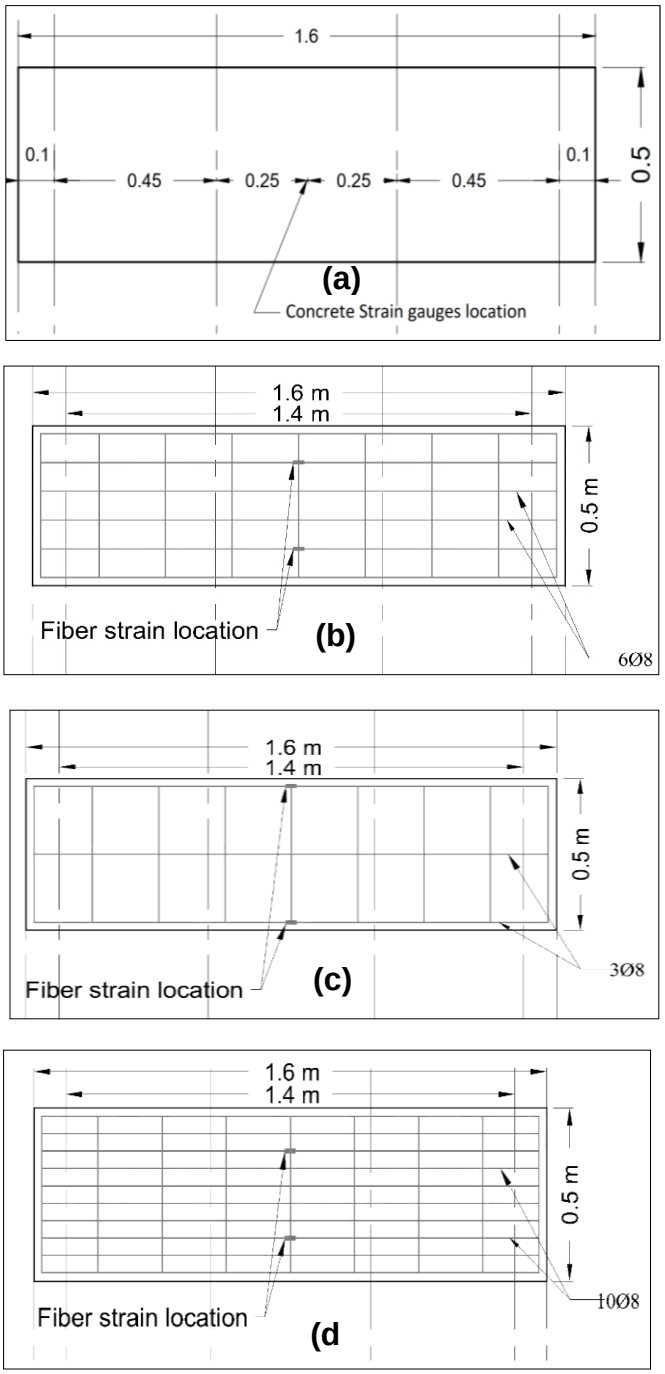

Figure 13 Locations of strain gauges: (a) on the concrete surface for all slabs; (b) on the FRP bars of GROUP I; (c) on the FRP bars of S6; (d) on the FRP bars of S7

2. RESULTS AND DISCUSSIONS

2.1 Failure Mechanism

Figure 14 shows the crack progression in slabs S1–S7, where all specimens failed in the compression zone with cracks initiating at mid-span and extending toward the supports, forming inclined failure patterns. Higher reinforcement ratios, as in S7, resulted in narrower cracks, while lower reinforcement in S6 led to wider, more distributed cracks. S1 showed finer cracks than S2 and S3, and S5 had narrower cracks than S1. S6 experienced more extensive cracking than S5, whereas S7 had minimal visible cracks aside from one major crack with noticeable mortar crushing at failure. These results offer important insights for enhancing slab design.

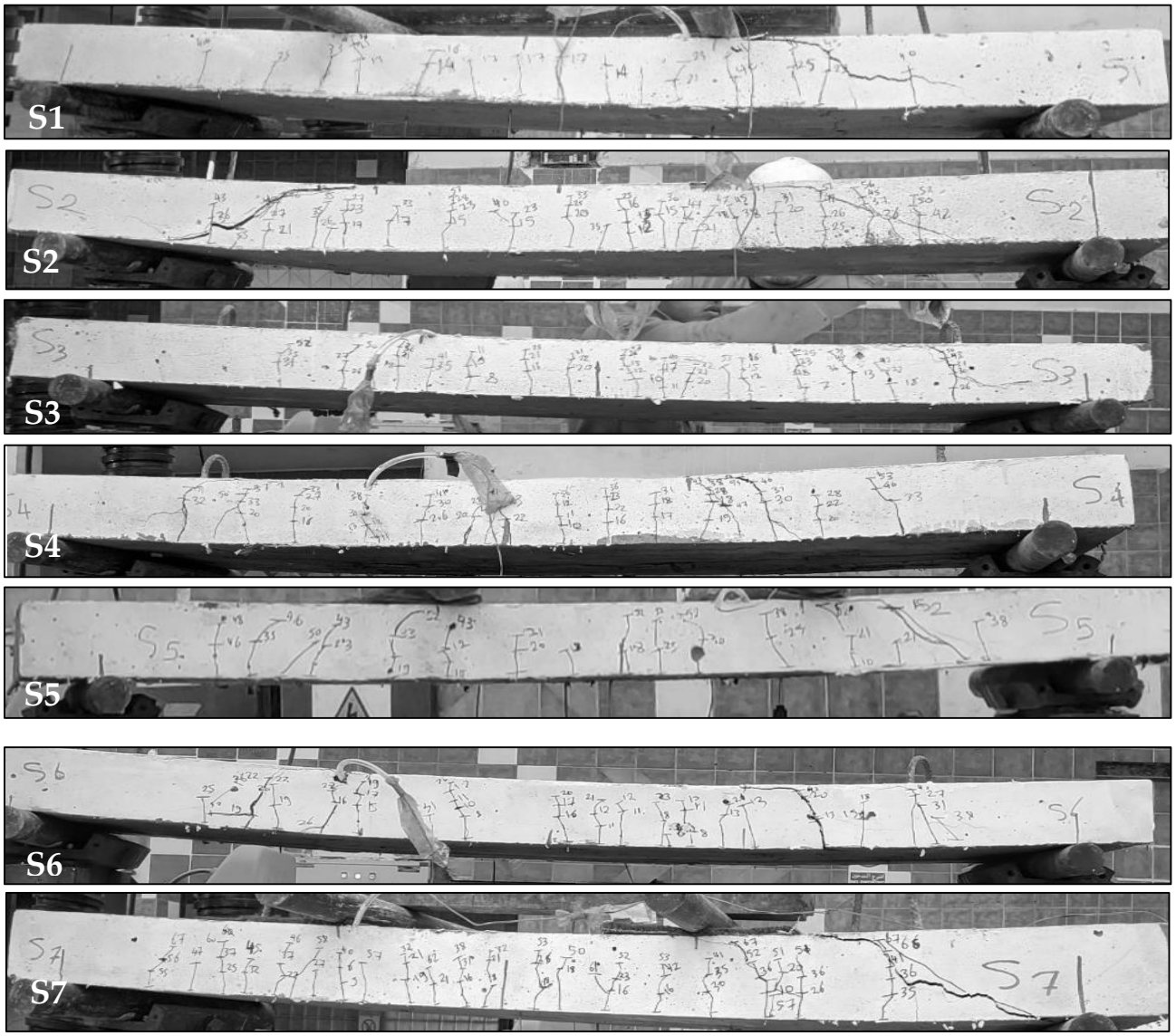

Figure 14 Cracks patterns of tested slabs

2.2 Cracking Load

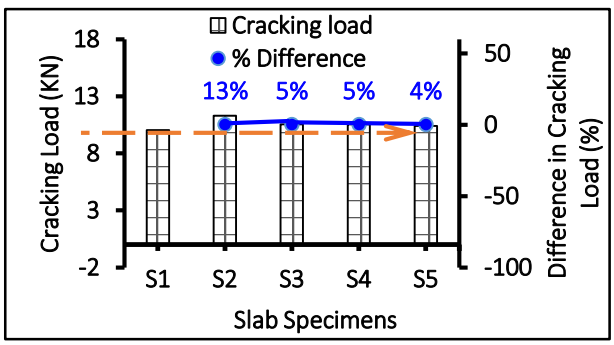

Figure 15a Cracking load for GROUP I

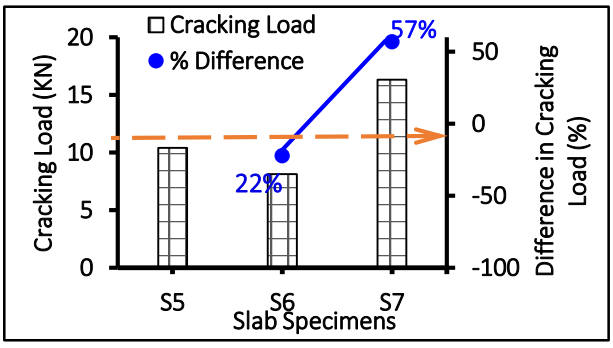

Figure 15b Cracking load for GROUP II

Figure 15 shows the first crack load results for all slabs. In GROUP I (**Figure 15a**), using seawater reduced the cracking load compared to the control slab S1 (14 kN). S2 dropped by 14.3% (12 kN), while S3, S4, and S5 each showed a 29% reduction (10 kN). In GROUP II (**Figure 15b**), with all slabs using seawater, reducing reinforcement in S6 lowered the cracking load by 20% (8 kN) compared to S5 (10 kN), while increasing reinforcement in S7 raised it by 60% (16 kN).

2.3 Flexural strength

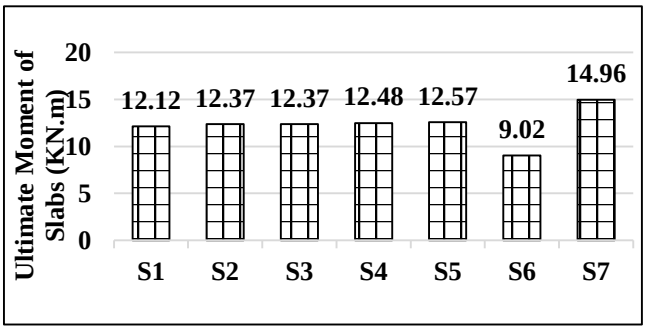

Figure 16 Ultimate moment capacity of slabs

2.4 Strain of GFRP and mortar

Figure 17 and **Figure 18** shows the tension and compression strain for GFRP and Mortar respectively at the mid span of slab specimens, Group (1) specimens showed a very identical load-starin curve in compaire to refrence slab S1. However, Group (2) Specimens showed a dramatic change at which , tension strain For S6 a very steady inclinding without any fluctuation. Remarkably, S6 has higher strain values compared to the reference slab S5, likewise compression stain for S6 , inopposite S7 showed lower strain values at both tension and compression, relative to the reference slab S5.

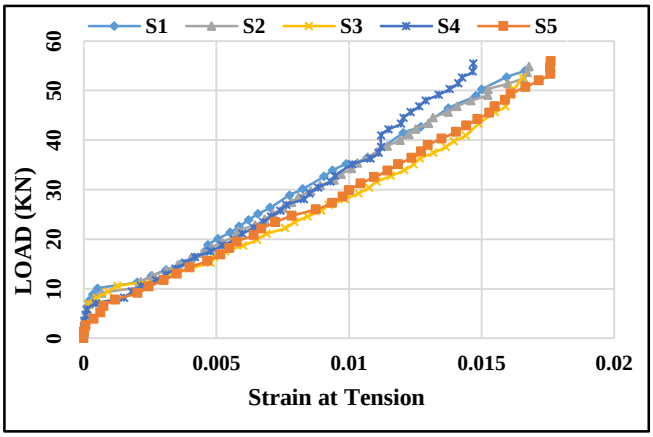

Figure 17a Load- Tension Strain Curves Slabs For Group I

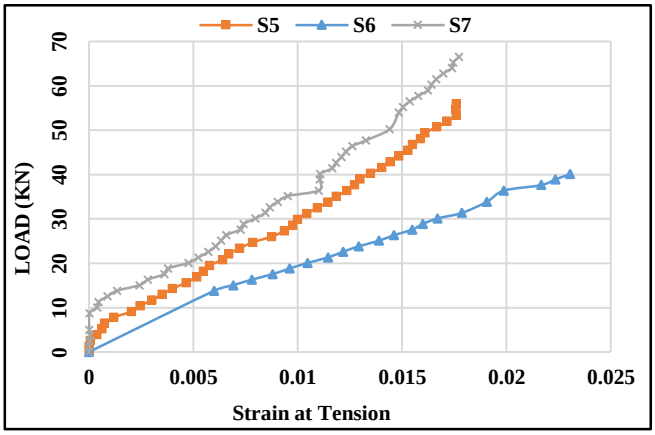

Figure17b load- tension strain curves Slabs for GROUP II

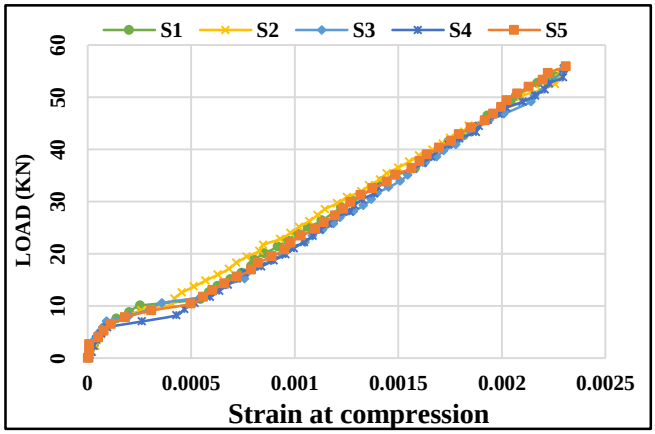

Figure 18a load- compression strain curves Slabs for GROUP I

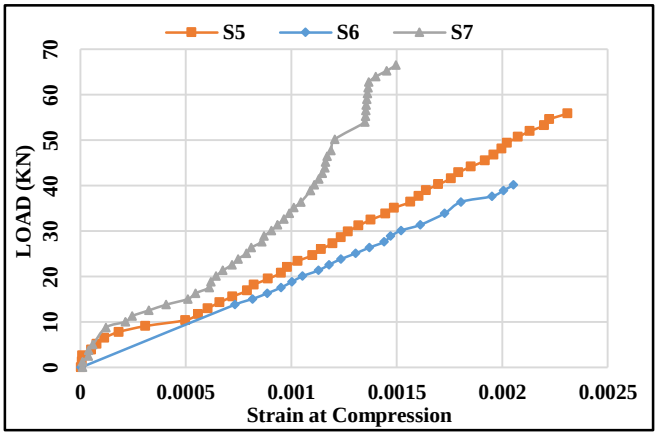

Figure 18b load- compression strain curves Slabs for GROUP II

2.5 Slab stiffness and toughness

Table 8 Experimental Test Results

Slab ID	Cracking Stage		Failure Stage		Stiffness (kN/mm)	Toughness (kN.mm)
	P_{cr} (kN)	Δ_{cr} (mm)	P_u (kN)	Δ_{max} (mm)		
S1	10.04	3.1	53.97	50.15	3.2	1555.1
S2	11.3	6.35	53.66	48.33	1.8	1439.7
S3	10.53	3.98	54.98	47.71	2.6	1399.7
S4	10.53	3.38	55.45	46.44	3.1	1457.6
S5	10.4	6.47	55.96	44.23	1.6	1251.7
S6	8.13	7.5	40.16	67.03	1.1	1638.7
S7	16.32	7.26	66.52	41.94	2.2	1523.1

P_{cr}: first crack load, Δ_{cr}: deflection at first crack, P_{max}: ultimate load, Δ_{max}: max deflection

2.6 Load – Deflection curves

Figure 19 Shows load –deflection for slabs (a and b) shows the load – deflection curves of the tested slabs, Group(1) presented in **Figure 19a** Load deflection curves have almost the same profile for all slabs where curves were steep and after the first crack, the curves took a curve shape till the end of loading before the failure load. However, Group(2) presented in **Figure 19b**, As loading increased, cracks formed and widened, extending to the slab's top and reducing stiffness. In Group 1 (S1-S5) with seawater (SW) mixing, failure loads slightly increased (1.6–3.57%) but with greater deflection as fiber bars resisted more load. For Group 2 (S6-S7) with different reinforcement ratios, S6 showed a 39.4% lower failure load (more deflection, fewer bars) while S7 achieved a 15.43% higher load capacity (less deflection, more bars), demonstrating how reinforcement quantity critically governs both strength and deformation behavior.

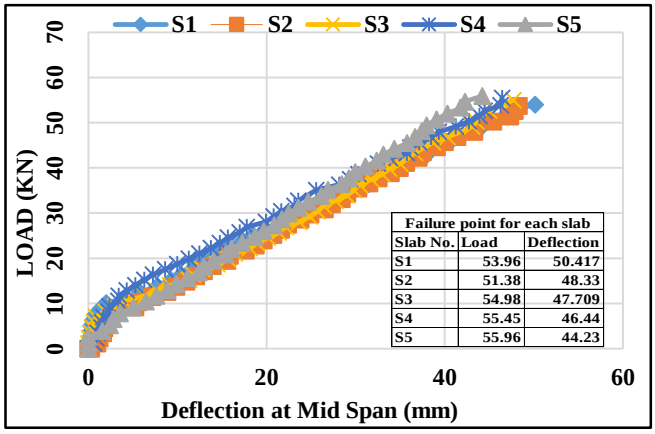

Figure 19a Slabs with different Sea- potable water ratios

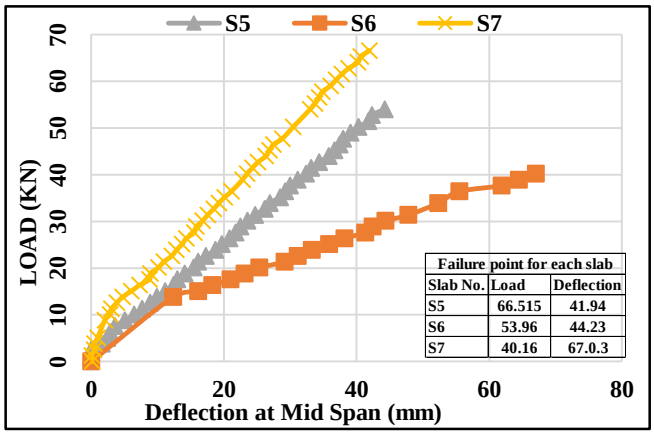

Figure 19b Slabs with different Reinforcement

Validation of theoretical analysis

Table 9 Shows the predicted ultimate moment is calculated with equation 1 according to ECP208 [23] and calculated with equation 2 according to ACI 440 [24] as compression controlled section cases based on ECP 208 design philosophy. For slabs with equal reinforcement ratios, the ultimate moment of the FC slab with 100% seawater (S5) was 3.57% higher than that with 0% seawater (S1). The experimental-to-predicted ultimate moment ratios ranged from 1.166 to 1.221 (avg. 1.214) using ECP 208, and from 0.885 to 0.961 (avg. 0.936) using ACI 440. For slabs with different reinforcement ratios, the average ratio was 1.18 (ECP 208) and 0.914 (ACI 440). These results suggest ACI 440 offers more consistent and conservative predictions, making it preferable for designing FC slabs reinforced with GFRP bars or other compression-controlled sections.

$a = \frac{\frac{f^*_{fe} A_f}{\gamma_f}}{(\frac{0.67 f_{cu}}{\gamma_c})b}$ (1-a) $M_u = A_F x \frac{f^*_{fe}}{\gamma_f} x \left(d - \frac{a}{2}\right)$ (1-b)	*Where:* M_u *= Theoretical ultimate moment (KN.m)* f^*_{FE} *= The design stress of the FRP bars including the effect of environmental factors (MPa)* A_f *= Main fiber Area (mm²),* *d = effective depth of slab (mm),* *a = Mortar compression zone depth (mm),nm* *b = slab width (mm).*
$M_n = A_f f_f \left(d - \frac{a}{2}\right)$ (2-a) $f_f = \sqrt{\frac{(E_f \varepsilon_{cu})^2}{4} + \frac{0.85 \beta_1 f'_c}{\rho_f} E_f \varepsilon_{cu}} - 0.5 E_f \varepsilon_{cu} \leq f_u$ (2-b) $a = \frac{A_f f_f}{0.8 f'_c b}$ (2-c) $\beta_1 = 0.85 - \frac{0.05 (f'_c - 28)}{7} \geq 0.65$ (2-d)	*Where:* *Mn = Unfactored Theoretical nominal moment (KN.m),* f'_c *= Cylinder compressive strength of concrete (MPa)* β_1 *= ratio distance from neutral axis to extreme tension fiber* ρ_f *= fiber reinforcement ratio*

Table 9 Experimental and theoretical ultimate moments of tested slabs

Specimens	M_{exp}	M_u (KN.m)"ECP208"		M_n (KN.m)"ACI 440"	
		M_{theo}	M_{exp} / M_{theo}	M_{theo}	M_{exp} / M_{theo}
S1	12.12	10.1	1.2	13.7	0.885
S2	12.37	10.14	1.219	13.1	0.944
S3	12.37	10.16	1.217	12.98	0.953
S4	12.48	10.26	1.215	13.28	0.939
S5	12.57	10.29	1.221	13.08	0.961
S6	9.02	7.73	1.166	9.83	0.917
S7	14.96	12.52	1.194	16.42	0.911

M_{exp}: Experimental results M_{theo}: Predicted results.

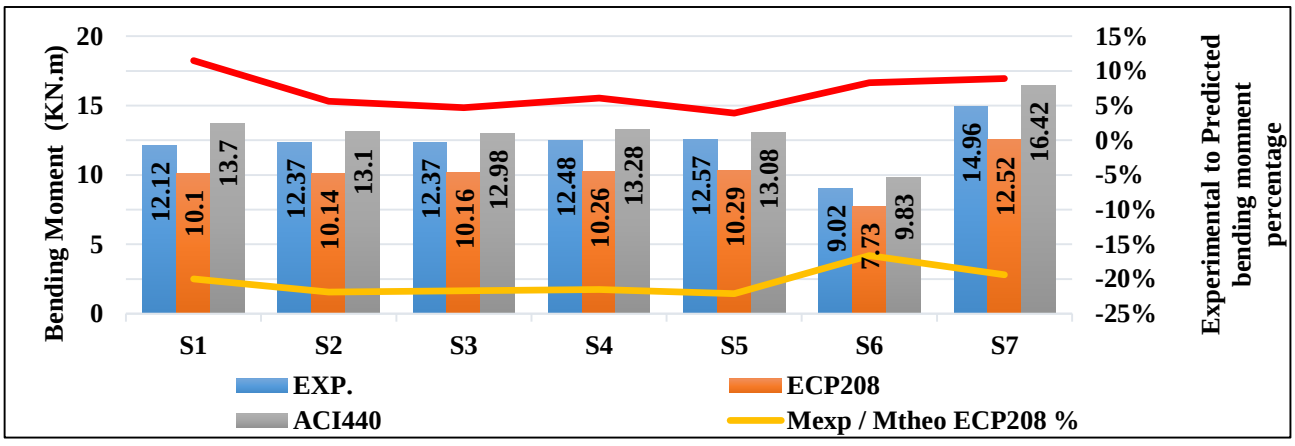

Figure 20 The comparison of bending moment values and their validation through theoretical analysis.

The results in **Table 9** and **Figure 20** showed that the theoretical ultimate moment result from using ECP208 [23] were higher than the experimental results by a Factor of 1.2 (20 %) on average in opposite using ACI 440 [24] showed slightly less values than experimental results on average by a Factor of 0.93 (7%.).

3. CONCLUSIONS

This study examines how varying SW–PW ratios and rebar ratio affect the flexural behavior of GFRP-reinforced FC slabs, based on specific dimensions and loading conditions. Key findings are summarized below:

1. Using seawater in the mortar mix lowered the water-to-cement (W/C) ratio, which reduced the initial slump values due to the presence of dissolved salts that affect flowability. Slump decreased by 1.81%, 4.54%, and 7.27% in mixes M3, M4, and M5 compared to the control mix M1 with potable water.
2. At 28 days, seawater mixes showed improved mechanical properties, with compressive and tensile strength increasing by 4% and 7.27% respectively compared to the potable water mix. This suggests seawater does not negatively impact early-age strength and may enhance cement hydration under certain conditions.
3. Seawater use led to higher ultimate loads in reinforced ferrocement slabs. Although cracking loads showed slight variation, slabs with higher reinforcement ratios experienced significant improvements in both cracking and ultimate loads due to increased section stiffness and load resistance.
4. Slabs with seawater exhibited lower deflection under the same loading compared to those with potable water, indicating better stiffness. Crack distribution was slightly affected by seawater, but reinforcement ratio played a larger role—lower reinforcement led to wider, more numerous cracks, while higher reinforcement reduced crack width and spacing.
5. Analytical predictions using ACI 440 closely matched experimental results, indicating better reliability compared to ECP 208, which showed larger deviations in estimating the behavior of ferrocement slabs with seawater and polymer reinforcement.

4. RECOMMENDATIONS

1. Investigate various seawater ratios and their long-term effects on Ferrocement with glass fiber.
2. Study flexural and shear behavior using different polymer reinforcements.
3. Explore alternative loading modes and performance under thermal exposure.

REFERENCES

[1] "Ferrocement 6: Lambot Symposium (Proceedings of Sixth International Symposium on Ferrocement): Antoine E. Naaman."

[2] G. Batson, "Ferrocement and laminated cementitious composites," Mater. Struct., vol. 33, no. 2, pp. CO3–CO3, 2000, doi: 10.1007/bf02484171.

[3] A. C. I. Committee 549, "549R-18: Report on Ferrocement," 2018.

[4] D. C. • Washington, "Ferrocement: Applications in Developing Countries NATIONAL ACADEMY OF SCIENckJBRARY," 1973.

[5] "Ferrocement: Proceedings of the Fifth International Symposium - Google Books."

[6] I. G. Shaaban, Y. B. Shaheen, E. L. Elsayed, O. A. Kamal, and P. A. Adesina, "Flexural characteristics of lightweight ferrocement beams with various types of core materials and mesh reinforcement," Constr. Build. Mater., vol. 171, pp. 802–816, 2018, doi: 10.1016/j.conbuildmat.2018.03.167.

[7] H. El-Hassan, T. El-Maaddawy, A. Al-Sallamin, and A. Al-Saidy, "Performance evaluation and microstructural characterization of GFRP bars in seawater-contaminated concrete," Constr. Build. Mater., vol. 147, pp. 66–78, Aug. 2017, doi: 10.1016/J.CONBUILDMAT.2017.04.135.

[8] H. Mamdouh, A. M. Ali, M. A. Osman, A. F. Deifalla, and N. M. Ayash, "Effects of Size and Flexural Reinforcement Ratio on Ambient-Cured Geopolymer Slag Concrete Beams under Four-Point Bending," Build. 2022, Vol. 12, Page 1554, vol. 12, no. 10, p. 1554, Sep. 2022, doi: 10.3390/BUILDINGS12101554.

[9] A. W. Hago, K. S. Al-Jabri, A. S. Alnuaimi, H. Al-Moqbali, and M. A. Al-Kubaisy, "Ultimate and service behavior of ferrocement roof slab panels," Constr. Build. Mater., vol. 19, no. 1, pp. 31–37, Feb. 2005, doi: 10.1016/J.CONBUILDMAT.2004.04.034.

[10] S. A. Miller, A. Horvath, and P. J. M. Monteiro, "Impacts of booming concrete production on water resources worldwide," Nat. Sustain. 2018 11, vol. 1, no. 1, pp. 69–76, Jan. 2018, doi: 10.1038/s41893-017-0009-5.

[11] D. Vafaei, R. Hassanli, X. Ma, J. Duan, and Y. Zhuge, "Sorptivity and mechanical properties of fiber-reinforced concrete made with seawater and dredged sea-sand," Constr. Build. Mater., vol. 270, p. 121436, Feb. 2021, doi: 10.1016/J.CONBUILDMAT.2020.121436.

[12] M. Bazli, M. Heitzmann, and B. V. Hernandez, "Hybrid fibre reinforced polymer and seawater sea sand concrete structures: A systematic review on short-term and long-term structural performance," Constr. Build. Mater., vol. 301, p. 124335, Sep. 2021, doi: 10.1016/J.CONBUILDMAT.2021.124335.

[13] Y. Wei, J. Bai, Y. Zhang, K. Miao, and K. Zheng, "Compressive performance of high-strength seawater and sea sand concrete-filled circular FRP-steel composite tube columns," Eng. Struct., vol. 240, p. 112357, Aug. 2021, doi: 10.10 16/J.ENGSTRUCT.2021.112357.

[14] S. Li, S. Guo, Y. Yao, Z. Jin, C. Shi, and D. Zhu, "The effects of aging in seawater and SWSSC and strain rate on the tensile performance of GFRP/BFRP composites: A critical review," Constr. Build. Mater., vol. 282, p. 122534, May 2021, doi: 10.1016/J.CONBUILDMAT.2021.122534.

[15] U. Ebead, D. Lau, F. Lollini, A. Nanni, P. Suraneni, and T. Yu, "A review of recent advances in the science and technology of seawater-mixed concrete," 2021, doi: 10.1016/j.cemconres.2021.106666.

[16] M. Khatibmasjedi, S. Ramanathan, P. Suraneni, and A. Nanni, "Compressive Strength Development of Seawater-Mixed Concrete Subject to Different Curing Regimes," 2020, doi: 10.14359/51725973.

[17] S. Rathnarajan and P. Sikora, "Seawater-mixed concretes containing natural and sea sand aggregates-A review," 2023, doi: 10.1016/j.rineng.2023.101457.

[18] P. Sikora et al., "Seawater-Mixed Lightweight Aggregate Concretes with Dune Sand, Waste Glass and Nanosilica: Experimental and Life Cycle Analysis," Int. J. Concr. Struct. Mater., vol. 17, no. 1, pp. 1–19, Dec. 2023, doi: 10.1186/ S40069-023-00613-4/FIGURES/14.

[19] G. Reddy Babu, B. Madhusudana Reddy, and N. Venkata Ramana, "Quality of mixing water in cement concrete 'a review,'" Mater. Today Proc., vol. 5, no. 1, pp. 1313–1320, Jan. 2018, doi: 10.1016/J.MATPR.2017.11.216.

[20] M. A. Elrahman, S. Y. Chung, P. Sikora, T. Rucinska, and D. Stephan, "Influence of Nanosilica on Mechanical Properties, Sorptivity, and Microstructure of Lightweight Concrete," Mater. 2019, Vol. 12, Page 3078, vol. 12, no. 19, p. 3078, Sep. 2019, doi: 10.3390/MA12193078.

[21] B. S. EN, "197-1. Cement–Part 1: Composition, specifications and conformity criteria for common cements," London Eur. Comm. Stand., 2011.

[22] "ASTM C1116 : Standard Specification for Fiber-Reinforced Concrete and Shotcrete."

[23] ECP Committee, 208. Egyptian Code for Design and Construction of Concrete Structures (ECP 208-2007).; Housing and Building National Research Center: Cairo, Egypt. 2007.

[24] Aci 440R-07, "Report on Fiber-Reinforced Polymer (FRP) Reinforcement for Concrete Structures, ACI 440R-07," Normos, p. 348, 2007.